Forced vibration analysis of composite beams based on the variable separation method

María Infantes, Philippe Vidal, Rafael Castro-Triguero, Laurent Gallimard, Enrique García-Macías, Olivier Polit

María Infantes, Philippe Vidal, Rafael Castro-Triguero, Laurent Gallimard, Enrique García-Macías & Olivier Polit. Forced vibration analysis of composite beams based on the variable separation method, *Mechanics of Advanced Materials and Structures,* volume 28, N°6, pp. 618-634, 2021
DOI: 10.1080/15376494.2019.1578015

Forced vibration analysis of composite beams based on the variable separation method

María Infantes, Philippe Vidal, Rafael Castro-Triguero, Laurent Gallimard, Enrique García-Macías & Olivier Polit

1. Introduction

Considering the increasing applications of composite and sandwich structures in the industrial field due to their high specific strength and stiffness, it is important to develop advanced models to design with a good compromise between accuracy and computational costs. In this regard, accurate knowledge of deflection and stresses is required to take into account effects of the transverse shear deformation due to the low ratio of transverse shear modulus to axial modulus. Moreover, the transverse normal effect has to be included into the formulation for thick structures. In fact, all these aspects can play an important role on the behavior of structures in service, in particular on natural frequencies or on the harmonic behavior.

According to published research, various theories in mechanics for composite or sandwich structures have been developed. They can be classified as: (i) the equivalent single layer approach (ESL) where the number of unknowns is independent of the number of layers, but the transverse shear and normal stresses continuity at the interfaces between layers are often violated. The classical laminate theory (CLT) [1], the first order shear deformation theory [2–7], and higher order theories [8–11] can be distinguished. Some of these theories also include the transverse normal effect with non-constant polynomial expressions of the out-of-plane displacement [12]. While most of these approaches are based on a displacement formulation, mixed formulations are also carried out in [13, 14] with the finite element method; (ii) the layerwise approach (LW) where the number of degrees of freedom (dofs) depends on the number of layers. This theory aims at overcoming the restriction of the ESL concerning the discontinuity of out-of-plane stresses at the interface layers. In recent contributions, various orders of expansion for the in-plane displacement are chosen: trigonometric [15], linear [16], and so forth; (iii) Alternative zig-zag approach developed in order to improve the accuracy of ESL models avoiding the additional computational cost of LW approach. Based on physical considerations and after some algebraic transformations, the number of unknowns becomes independent of the number of layers. Global higher-order theories and the zig-zag theories are asses in [17] to predict the global response of soft-core sandwich beams. A family of models was employed in [18] and more recently improved in [19, 20] with different orders of kinematic assumptions, taking into account the transverse normal strain. Note also the refined approach based on the Sinus model [21–23]. An extended review work on these models can be found in reference [24].

It should be noted the systematic approach based on the Carrrera's Unified Formulation to provide a large amount of two-dimensional (2D) models for composite structures based on ESL and/or LW descriptions of the unknowns [25–27]. The aforementioned works deal with only some aspects of the broad research activity about models for layered structures and corresponding finite element formulations. An extensive assessment of different approaches has been made in [24, 28–32]. A survey of developments in the vibration analysis of laminated composite beams is compiled in [33].

Over the past years, the proper generalized decomposition (PGD) has shown interesting features in the reduction model framework [34]. This type of method was introduced by Ladevèze [35] and called "radial approximation" in the

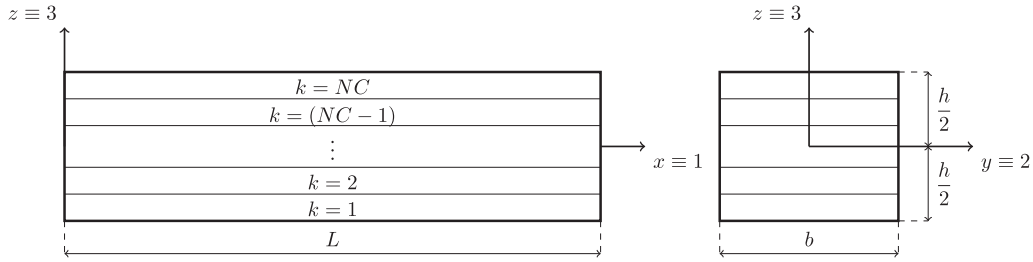

Figure 1. The laminated beam and coordinate system.

Table 1. Table of principal notation.

Ω_x	Problem domain in beam axis direction	N	Number of total enrichment steps
Ω_z	Problem domain in thickness direction	$[q^v]$	Vector of dofs associated with the mesh on Ω_x
ω	Load frequency	$[q^f]$	Vector of dofs associated with the mesh on Ω_z
Ω	Dimensionless load frequency	$[g]$	Vector of dofs associated with the mesh on ω
NC	Number of layers	n_x	Number of elements in the mesh on Ω_x
L	Length of the beam	n_z	Number of elements in the mesh on Ω_z
h, h_f, h_c	Thickness of the beam, face, and core	n_ω	dofs associated with the mesh on ω
$S = \frac{L}{h}$	Length to thickness ratio	$Ndof_x$	dofs associated with the mesh on Ω_x
		$Ndof_z$	dofs associated with the mesh on Ω_z

framework of the LArge Time INcrement (LATIN) method. In this latter, space coordinates and time variables are separated. It allows to decrease drastically computational time such as in [36, 37]. It has been also used in the context of separation of coordinate variables in multi-dimensional PDEs [34]. In particular, it has been applied for composite beams and plates in [38–41] with an in-plane/out-of-plane coordinate separation. Separated representation can be also applied to deduce parametric solutions where parameters are considered as problem extra-coordinates, see for example [42]. For a review about the PGD and its fields of application, readers can refer to [43, 44].

In this work, a model based on the proper generalized decomposition method is built for the forced vibration problem of laminated and sandwich beams under harmonic excitation. For this purpose, the displacements are written under the form of separated variable representation, that is a sum of products of unidimensional functions of x and z coordinates, and also the pulsation of the harmonic load ω. Note that the space and load frequency variable separation has been already addressed in [45]. Nevertheless, herein also the in-plane/out-of-plane coordinate separation is included in the formulation as it is well-suited to perform efficient computations for composite structures in terms of model complexity and computational cost. Moreover, the deduced explicit solution with respect to the pulsation allows us to avoid numerous classical computations for each considered value of the load frequency within the domain of interest. To achieve that, the approximation of the 2D beam is based on a quadratic finite element (FE) approximation for the variation with respect to x and a quadratic LW description for the variation with respect to z. Using the PGD, each unknown function of x is classically approximated using one dof at each node of the mesh while the LW unknown functions of z are global for the whole beam. Finally, the deduced non-linear problem implies the resolution of three linear problems alternatively. This process yields to few unknowns involved in each of these linear problems.

In this paper, the reference problem is firstly recalled in Section 2. The application of the PGD is given in the framework of the forced vibration problems with a specific parametrization in Section 3. This particular assumption on the displacements yields a nonlinear problem, solved through a classical iterative process. In Section 4, the FE discretization is also described. Finally, the algorithm derived in the paper is verified numerically in Section 5. For this purpose, a preliminary convergence study is first carried out. Then, the method is illustrated by numerical tests which have been performed upon various laminated and sandwich beams. The influence of slenderness ratios and boundary conditions are addressed. The accuracy of computations is evaluated by comparisons with an exact 2D elasticity solution, 2D computations using commercial finite element software and also results available in the literature. It is shown that the method allows us to obtain both the frequency response function, and the shape modes with the associated eigen frequencies with very good agreement respect to the reference solutions by using a dimensionally-reduced model which supposes less computational cost.

2. Reference problem description

In the present study, a straight beam of length L with a rectangular uniform cross section of thickness h and depth b is considered. The beam consists of NC layers assumed to be orthotropic in the beam axes. The x axis is taken along the longitudinal beam axis whereas y and z are the two axes of symmetry of the rectangular cross section (see Figure 1). The principal notation used in the formulation of the problem is summarized in Table 1.

Hereafter, the y coordinate is neglected and the beam is considered in the (x, z) plane, that is, in the domain $\Omega = \Omega_x \times \Omega_z = [0 \leq x \leq L] \times [-\frac{h}{2} \leq z \leq \frac{h}{2}]$. In classical beam theory, the displacement field is assumed to be expressed as

$$[u] = \begin{bmatrix} u_1(x,z) \\ u_3(x,z) \end{bmatrix} = \begin{bmatrix} \sum_{i=0}^{N_1} z^i v_1^i(x) \\ \sum_{i=0}^{N_3} z^i v_3^i(x) \end{bmatrix} \tag{1}$$

where $(v_1^i(x), v_3^i(x))$ are functions to be sought and N_1, N_3 are integers. For instance, by using this expression, models found in the literature can be described as follows

- The classical Timoshenko models with N_1=1 and N_3=0,
- ED2 model in Carrera's unified formulation [30] with N_1=2 and N_3=2.

2.1. Governing equations

The problem of a composite beam subjected to an arbitrary dynamic excitation $[F_d(t)]$ is considered. Stresses can be conveniently written under the following form:

$$[\sigma]^\top = [\sigma_{11} \quad \sigma_{33} \quad \sigma_{13}] \qquad \text{or} \qquad [\tau] = \begin{bmatrix} \sigma_{11} & \sigma_{13} \\ \sigma_{13} & \sigma_{33} \end{bmatrix} \tag{2}$$

The boundary value problem to be solved consists of finding the displacement $[u(M,t)]$ and stress $[\sigma(M,t)]$, $M \in \Omega$ such that

$$[\nabla_S]^\top [\sigma] + [b] = \rho \frac{\partial^2 [u]}{\partial t^2}, \quad \text{on} \quad \Omega \tag{3}$$

$$[\tau(M,t)][n] = [F_d(t)], \quad \forall M \in \partial_F \Omega \tag{4}$$

$$[u(M,t)] = [u_d(t)], \quad \forall M \in \partial_u \Omega \tag{5}$$

where $[u_d]$ represents the displacement boundary condition, $[n]$ is the normal vector at the load application point, $[F_d(t)]$ is the prescribed surface load applied on $\partial_F \Omega = \partial_F \Omega_x \times \partial_F \Omega_z$, $[b]$ is the prescribed body load, ρ is the density of the material and $[\nabla_S]$ is the operator

$$[\nabla_S]^\top = \begin{bmatrix} \frac{\partial}{\partial x} & 0 & \frac{\partial}{\partial z} \\ 0 & \frac{\partial}{\partial z} & \frac{\partial}{\partial x} \end{bmatrix} \tag{6}$$

The problem can be expressed only in terms of the displacements using the constitutive relation $[\sigma] = [C][\varepsilon]$ and the kinematics equations $[\varepsilon] = [\nabla_S][u]$.

2.1.1. Constitutive relation

Each layer of the beam is assumed to be orthotropic. The stress–strain law of the kth layer is

$$\begin{bmatrix} \sigma_{11}^{(k)} \\ \sigma_{33}^{(k)} \\ \sigma_{13}^{(k)} \end{bmatrix} = \begin{bmatrix} \bar{C}_{11}^{(k)} & \bar{C}_{13}^{(k)} & 0 \\ \bar{C}_{13}^{(k)} & \bar{C}_{33}^{(k)} & 0 \\ 0 & 0 & \bar{C}_{55}^{(k)} \end{bmatrix} \begin{bmatrix} \varepsilon_{11}^{(k)} \\ \varepsilon_{33}^{(k)} \\ \gamma_{13}^{(k)} \end{bmatrix} \tag{7}$$

where $\bar{C}_{ij}^{(k)}$ are the elastic moduli of the material taking into account the zero transverse normal stress hypothesis (σ_{22}=0) expressed by

$$\bar{C}_{ij}^{(k)} = C_{ij}^{(k)} - C_{i2}^{(k)} C_{j2}^{(k)} / C_{22}^{(k)}, \quad i,j = 1,3 \tag{8}$$

$$\bar{C}_{55}^{(k)} = C_{55}^{(k)} \tag{9}$$

where $C_{ij}^{(k)}$ are the 3D stiffness coefficients.

2.1.2. Classical variational formulation of the boundary value problem

Regarding the time dependent excitation, it can be expressed as $[F_d(t)] = [f_d] \cdot g(t)$, with $||f_d|| = 1$. The function $g(t)$ can be formulated as a superposition of weighted harmonic functions $e^{i\omega t}$, being i the imaginary unit and ω the load angular frequency

$$g(t) = \int_{-\infty}^{\infty} G(\omega)\ e^{i\omega t} \mathrm{d}\omega \tag{10}$$

where $G(\omega)$ is the Fourier transform of $g(t)$ and it represents the content of each harmonic in the excitation.

In the following, a single harmonic excitation, $[F_d(t)] = [f_d]\ e^{i\omega t}$, is assumed as a basic problem. The response of a linear solid in absence of body loads and subjected to a harmonic excitation is presumed to have the same frequency as the applied load, $[u(M,t)] = [u(M)]e^{i\omega t}$, with $[u(M)]$ containing the displacements amplitude. Under these assumptions and with U the space of admissible displacement, the classical variational principle of a beam subjected to a harmonic load can be expressed as:

$$\text{find } [u(M)] \in U \text{ such that}$$

$$\int_\Omega [\varepsilon(\delta u)]^\top [\sigma(u)]\ \mathrm{d}V - \int_{\partial_F \Omega} [\delta u]^\top [f_d]\ \mathrm{d}S = \omega^2 \int_\Omega \rho [\delta u]^\top [u]\ \mathrm{d}V, \quad \forall\ [\delta u] \in \delta U \tag{11}$$

where $[f_d]$ is the amplitude of the harmonic load. Note that in Equation (11), damping is not considered.

3. Application of the proper generalized method to forced vibration beam

The PGD was introduced in [46]. This method is based on an *a priori* construction of the solution in separate variables. In the literature, the PGD has been used in order to separate spatial variables and also to consider problem parameters as extra-coordinates. In this approach, the PGD is first used to considering both the spatial variable separation and the introduction of the load frequency as an extra-coordinate in the solution. The following sections are dedicated to the application of PGD to the previous described problem.

3.1. Displacement field hypothesis

The displacement solution is built as

$$\begin{bmatrix} u_1(x,z,\omega) \\ u_3(x,z,\omega) \end{bmatrix} = \sum_{i=1}^{N} [u^i] = \sum_{i=1}^{N} g^i(\omega) \begin{bmatrix} f_1^i(z) & v_1^i(x) \\ f_3^i(z) & v_3^i(x) \end{bmatrix} \tag{12}$$

where $g^i(\omega), f_1^i(z), f_3^i(z), v_1^i(x), v_3^i(x)$ are functions which must be computed during the resolution process for each enrichment step $i = 1, 2, ..., n, ..., N$.

3.1.1. New variational formulation of the boundary value problem

Considering the expression of the displacement (Equation (12)), Equation (11) can be solved for a given value of the load frequency ω. Hence, the consideration of the load frequency within an interval $[\omega_{\min}, \omega_{\max}]$ involves the resolution of multiple problems for many values of ω. To avoid these numerous resolutions, a new formulation is proposed:

$$\text{find} \quad [u(M,\omega)] \in U \text{ such that}$$

$$\int_\omega \int_\Omega [\varepsilon(\delta u)]^\top [\sigma(u)] \, dV \, d\omega - \int_\omega \int_{\partial_F \Omega} [\delta u]^\top [f_d] \, dS \, d\omega = \int_\omega \int_\Omega \omega^2 \rho [\delta u]^\top [u] \, dV \, d\omega, \quad \forall \, [\delta u] \in \delta U \tag{13}$$

3.2. The problem to be solved

Equation (12) can be written in a more compact form as

$$[u] = \sum_{i=1}^{N} g^i [F^i][v^i] = \sum_{i=1}^{N} g^i [V^i][f^i] \tag{14}$$

where

$$[v^i] = \begin{bmatrix} v_1^i(x) \\ v_3^i(x) \end{bmatrix}, \quad [f^i] = \begin{bmatrix} f_1^i(z) \\ f_3^i(z) \end{bmatrix} \tag{15}$$

and

$$[V^i] = \begin{bmatrix} v_1^i(x) & 0 \\ 0 & v_3^i(x) \end{bmatrix}, \quad [F^i] = \begin{bmatrix} f_1^i(z) & 0 \\ 0 & f_3^i(z) \end{bmatrix} \tag{16}$$

In view of the above equations, an iterative procedure must be introduced. Assuming that the first $(n-1)$ functions have already been computed, the solution for iteration n is

$$[u] = [\bar{u}] + g[V][f] = [\bar{u}] + g[F][v] \tag{17}$$

where $[\bar{u}]$ is the displacement solution at iteration $(n-1)$ defined by

$$[\bar{u}] = \sum_{i=1}^{n-1} [u^i] = \sum_{i=1}^{n-1} g^i [F^i][v^i] = \sum_{i=1}^{n-1} g^i [V^i][f^i] \tag{18}$$

Note that for sake of clarity the superscript n is ignored for the current unknowns (g, f, v). These functions are computed such that Equation (17) satisfies the weak form in Equation (13). By ordering the terms and taking into account the constitutive law in the mentioned weak form

$$\int_\omega \int_\Omega [\varepsilon(\delta u)]^\top [C][\varepsilon(u)] \, dV \, d\omega - \int_\omega \int_\Omega \omega^2 [\delta u]^\top [u] \, dV \, d\omega = \int_\omega \int_{\partial_F \Omega} [\delta u]^\top [f_d] \, dS \, d\omega \tag{19}$$

where $[C]$ represents the plane stress-reduced stiffness tensor of each layer k as in Equation (7) and δu is the virtual displacement

$$[\delta u] = \delta g[F][v] + g[V][\delta f] + g[F][\delta v] = \delta u_\omega + \delta u_f + \delta u_v \tag{20}$$

Introducing Equation (20) into Equation (19) the problem is decomposed into three equations, which are

$$\int_\omega \int_\Omega \Big([\varepsilon(\delta u_\omega)]^\top [C][\varepsilon(\bar{u} + g \; F \; v)] - \omega^2 \rho [\delta u_\omega]^\top ([\bar{u}] + g[F][v]) \Big) \, dV \, d\omega = \int_\omega \int_{\partial_F \Omega} [\delta u_\omega]^\top [f_d] \, dS \, d\omega \tag{21}$$

$$\int_\omega \int_\Omega \Big([\varepsilon(\delta u_f)]^\top [C][\varepsilon(\bar{u} + g \; V \; f)] - \omega^2 \rho [\delta u_f]^\top ([\bar{u}] + g[V][f]) \Big) \, dV \, d\omega = \int_\omega \int_{\partial_F \Omega} [\delta u_f]^\top [f_d] \, dS \, d\omega \tag{22}$$

$$\int_\omega \int_\Omega \Big([\varepsilon(\delta u_v)]^\top [C][\varepsilon(\bar{u} + g \; F \; v)] - \omega^2 \rho [\delta u_v]^\top ([\bar{u}] + g[F][v]) \Big) \, dV \, d\omega = \int_\omega \int_{\partial_F \Omega} [\delta u_v]^\top [f_d] \, dS \, d\omega \tag{23}$$

As these equations define a coupled nonlinear problem, a non-linear resolution strategy must be used. The fixed point method is the simplest one. At the first step, initial functions $g^{(0)}$ and $f^{(0)}$ are set, and $v^{(0)}$ is computed from Equation (23) with $g = g^{(0)}$ and $f = f^{(0)}$. Then, at each iteration, the algorithm computes a new solution $g^{(m+1)}, f^{(m+1)}, v^{(m+1)}$ such that

- Step 1: $g^{(m+1)}$ satisfies Equation (21) for f, v set to $f^{(m)}, v^{(m)}$
- Step 2: $f^{(m+1)}$ satisfies Equation (22) for g, v set to $g^{(m+1)}, v^{(m)}$
- Step 3: $v^{(m+1)}$ satisfies Equation (23) for g, f set to $g^{(m+1)}, f^{(m+1)}$

The algorithm proceeds iteratively until reaching a fixed point.

3.2.1. Variational problem defined on load frequency domain ω

In order to simplify the notation, the functions $f^{(m)}, v^{(m)}$, which are assumed to be known, will be denoted as $\tilde{f}, \tilde{v}$ (and subsequently $\tilde{F}, \tilde{V}$ in matrix form) and the function $g^{(m+1)}$ to be computed will be denoted as g. The functions $\bar{g}^i, \bar{f}^i, \bar{v}^i$ are the solutions at the previous enrichment steps $i = 1, 2, ..., (n-1)$. The strain in Equation (21) is defined in matrix notation as

$$[\varepsilon(g \; \tilde{F} \; \tilde{v})] = g \left[\Sigma_z(\tilde{f})\right] [\tilde{\mathcal{E}}_v] \tag{24}$$

with

$$\left[\Sigma_z(\tilde{f})\right] = \begin{bmatrix} 0 & \tilde{f}_1 & 0 & 0 \\ 0 & 0 & \tilde{f}_3' & 0 \\ \tilde{f}_1' & 0 & 0 & \tilde{f}_3 \end{bmatrix}$$

$$\text{and} \quad \left[\tilde{\mathcal{E}}_v\right]^\top = \left[\tilde{v}_1 \quad \tilde{v}_1' \quad \tilde{v}_3 \quad \tilde{v}_3'\right] \tag{25}$$

where the prime ($'$) stands for the classical derivation. Thus, the variational problem defined on ω from Equation (21) is then

$$g = \frac{f_\omega\left(\tilde{f},\tilde{v}\right) + \omega^2 \ \sum_{i=1}^{n-1} \bar{g}^i \mu_\omega^i\left(\tilde{f},\tilde{v},\bar{u}\right) - \sum_{i=1}^{n-1} \bar{g}^i \sigma_\omega^i\left(\tilde{f},\tilde{v},\bar{u}\right)}{k_\omega\left(\tilde{f},\tilde{v}\right) - \omega^2 m_\omega\left(\tilde{f},\tilde{v}\right)},$$

$$\forall \quad \omega \in [\omega_{min}, \omega_{max}] \tag{26}$$

with

$$k_\omega\left(\tilde{f},\tilde{v}\right) = \int_\Omega \left[\tilde{\mathcal{E}}_v\right]^\top \left[\Sigma_z\left(\tilde{f}\right)\right]^\top \ [C] \ \left[\Sigma_z\left(\tilde{f}\right)\right] \ \left[\tilde{\mathcal{E}}_v\right] \ \mathrm{d}V \tag{27}$$

$$\sigma_\omega^i\left(\tilde{f},\tilde{v},\bar{u}\right) = \int_\Omega \left[\tilde{\mathcal{E}}_v\right]^\top \left[\Sigma_z\left(\tilde{f}\right)\right]^\top \ [C] \ \left[\Sigma_z\left(\overline{f^i}\right)\right] \left[\overline{\mathcal{E}_v^i}\right] \ \mathrm{d}V \tag{28}$$

$$m_\omega\left(\tilde{f},\tilde{v}\right) = \int_\Omega [\tilde{v}]^\top \ [\tilde{F}]^\top \rho \ [\tilde{F}] \ [\tilde{v}] \ \mathrm{d}V \tag{29}$$

$$\mu_\omega^i\left(\tilde{f},\tilde{v},\bar{u}\right) = \int_\Omega [\tilde{v}]^\top \ [\tilde{F}]^\top \rho \ [\bar{F}^i] \ [\bar{v}^i] \ \mathrm{d}V \tag{30}$$

$$f_\omega\left(\tilde{f},\tilde{v}\right) = \int_{\partial_F\Omega} [\tilde{v}]^\top \ [\tilde{F}]^\top \ [f_d] \ \mathrm{d}S \tag{31}$$

By using the variational problem expression in Equation (21), the value of $g(\omega)$ can be calculated explicitly for any ω considered in the range $[\omega_{min}, \omega_{max}]$ through the Equation (26). Note that, as can be inferred from Equation (26), there are values of ω for which resonance is detected. These values ω_n are calculated at convergence as

$$\omega_n^2 = \frac{k_\omega}{m_\omega} \tag{32}$$

This value will be used to estimate the natural frequencies of the beam as it will be shown in Section 5 involving the numerical test cases.

3.2.2. Variational problem defined on Ω_z

The functions $g^{(m+1)}, v^{(m)}$, assumed to be known, will be denoted as $\tilde{g}, \tilde{v}$ and the function $f^{(m+1)}$ to be computed will be denoted as f. The strain in Equation (22) is defined in matrix notation as

$$\left[\varepsilon\left(\tilde{g} \ \ \tilde{V} \ f\right)\right] = \tilde{g} \ \left[\Sigma_x(\tilde{v})\right] \ \left[\mathcal{E}_f\right] \tag{33}$$

with

$$\left[\Sigma_x(\tilde{v})\right] = \begin{bmatrix} \tilde{v}_1' & 0 & 0 & 0 \\ 0 & 0 & 0 & \tilde{v}_3' \\ 0 & \tilde{v}_1 & \tilde{v}_3' & 0 \end{bmatrix}$$

$$\text{and} \quad \left[\mathcal{E}_f\right]^\top = \left[f_1 \quad f_1' \quad f_3 \quad f_3'\right] \tag{34}$$

Introducing the above expression into Equation (22), the variational problem defined on Ω_z is

$$\begin{aligned} &\gamma_\omega \int_{\Omega_z} \left[\delta\mathcal{E}_f\right]^\top [k_x(\tilde{v})] \ \left[\mathcal{E}_f\right] \ \mathrm{d}z - \alpha_\omega \int_{\Omega_z} [\delta f]^\top [m_x(\tilde{v})] \ [f] \ \mathrm{d}z \\ &= \beta_\omega \int_{\partial_F\Omega_z} [\delta f]^\top \left[f_x(\tilde{v})\right] \ \mathrm{d}z + \sum_{i=1}^{n-1} \alpha_\omega^i \int_{\Omega_z} [\delta f]^\top \left[\mu_x^i(\tilde{v},\bar{u})\right] \ \mathrm{d}z \\ &\quad - \sum_{i=1}^{n-1} \gamma_\omega^i \int_{\Omega_z} \left[\delta\mathcal{E}_f\right]^\top \left[\sigma_x^i(\tilde{v},\bar{u})\right] \ \mathrm{d}z \end{aligned} \tag{35}$$

where the coefficients α_ω and γ_ω only depend on the load frequency

$$\gamma_\omega = \int_\omega \tilde{g}^2 \mathrm{d}\omega \ ; \gamma_\omega^i = \int_\omega \tilde{g} \ \bar{g}^i \ \mathrm{d}\omega \tag{36}$$

$$\alpha_\omega = \int_\omega \omega^2 \tilde{g}^2 \mathrm{d}\omega \ ; \alpha_\omega^i = \int_\omega \omega^2 \tilde{g} \ \bar{g}^i \ \mathrm{d}\omega \tag{37}$$

$$\beta_\omega = \int_\omega \tilde{g} \mathrm{d}\omega \tag{38}$$

and

$$[k_x(\tilde{v})] = \int_{\Omega_x} [\Sigma_x(\tilde{v})]^\top \ [C] \ [\Sigma_x(\tilde{v})] \ \mathrm{d}x \tag{39}$$

$$\left[\sigma_x^i(\tilde{v},\bar{u})\right] = \int_{\Omega_x} [\Sigma_x(\tilde{v})]^\top \ [C] \ \left[\Sigma_x(\bar{v}^i)\right] \left[\overline{\mathcal{E}_f^i}\right] \ \mathrm{d}x \tag{40}$$

$$[m_x(\tilde{v})] = \int_{\Omega_x} [\tilde{V}]^\top \ \rho \ [\tilde{V}] \ \mathrm{d}x \tag{41}$$

$$\left[\mu_x^i(\tilde{v},\bar{u})\right] = \int_{\Omega_x} [\tilde{V}]^\top \ \rho \ [\bar{V}^i] \left[\overline{f^i}\right] \ \mathrm{d}x \tag{42}$$

$$\left[f_x(\tilde{v})\right] = \int_{\partial_F\Omega_x} [\tilde{V}]^\top \ [f_d] \ \mathrm{d}x \tag{43}$$

In this way, the variational problem defined by Equation (22) is a linear expression that must be solved in the Ω_z domain through Equation (35).

3.2.3. Variational problem defined on Ω_x

At this step, the functions $g^{(m+1)}, f^{(m+1)}$, which are assumed to be known, will be denoted as $\tilde{g}, \tilde{f}$ and the function $v^{(m+1)}$ to be computed will be denoted as v. The expression of the strain being $[\varepsilon(\tilde{g} \ \tilde{F} \ v)] = \tilde{g} \ [\Sigma_z(\tilde{f})] \ [\mathcal{E}_v]$, the variational problem defined on Ω_x becomes

$$\begin{aligned} &\gamma_\omega \int_{\Omega_x} [\delta\mathcal{E}_v]^\top \left[k_z\left(\tilde{f}\right)\right] \ [\mathcal{E}_v] \ \mathrm{d}x - \alpha_\omega \int_{\Omega_x} [\delta v]^\top \left[m_z\left(\tilde{f}\right)\right] \ [v] \ \mathrm{d}x \\ &= \beta_\omega \int_{\partial_F\Omega_x} [\delta v]^\top \left[f_z\left(\tilde{f}\right)\right] \ \mathrm{d}x + \sum_{i=1}^{n-1} \alpha_\omega^i \int_{\Omega_x} [\delta v]^\top \left[\mu_z^i\left(\tilde{f},\bar{u}\right)\right] \ \mathrm{d}x \\ &\quad - \sum_{i=1}^{n-1} \gamma_\omega^i \int_{\Omega_x} [\delta\mathcal{E}_v]^\top \left[\sigma_z^i\left(\tilde{f},\bar{u}\right)\right] \ \mathrm{d}x \end{aligned} \tag{44}$$

with

$$\left[k_z\left(\tilde{f}\right)\right] = \int_{\Omega_z} \left[\Sigma_z\left(\tilde{f}\right)\right]^\top \; [C] \; \left[\Sigma_z\left(\tilde{f}\right)\right] \; \mathrm{d}z \tag{45}$$

$$\left[\sigma_z^i\left(\tilde{f},\bar{u}\right)\right] = \int_{\Omega_z} \left[\Sigma_z\left(\tilde{f}\right)\right]^\top \; [C] \; \left[\Sigma_z\left(\overline{f^i}\right)\right]\left[\overline{\mathcal{E}_v^i}\right] \; \mathrm{d}z \tag{46}$$

$$\left[m_z\left(\tilde{f}\right)\right] = \int_{\Omega_z} [\tilde{F}]^\top \; \rho \; [\tilde{F}] \; \mathrm{d}z \tag{47}$$

$$\left[\mu_z^i\left(\tilde{f},\bar{u}\right)\right] = \int_{\Omega_z} [\tilde{F}]^\top \; \rho \; [\bar{F}^i][\bar{v}^i] \; \mathrm{d}z \tag{48}$$

$$\left[f_z\left(\tilde{f}\right)\right] = \int_{\partial_F\Omega_z} [\tilde{F}]^\top \; [f_d] \; \mathrm{d}z \tag{49}$$

Analogously, the variational problem defined by Equation (23) is a linear expression that must be solved in the Ω_x domain through Equation (44).

4. Galerkin discretization

To build the displacement solution, a discrete representation of the functions g, f, v must be introduced. A classical finite element approximation is used in Ω_x and Ω_z. The element vector of dofs associated with the finite element mesh in Ω_x and Ω_z are denoted as $[q_e^v]$ and $[q_k^f]$, respectively. The part of the displacement and strain fields that only depends on spatial variables are determined from the values of $[q_e^v]$ and $[q_k^f]$ by

$$\begin{aligned} [v_e] &= [N_x]\left[q_e^v\right]; \quad \left[\mathcal{E}_v^e\right] = [B_x]\left[q_e^v\right]; \\ [f_k] &= [N_z]\left[q_k^f\right]; \quad \left[\mathcal{E}_f^k\right] = [B_z]\left[q_k^f\right] \end{aligned} \tag{50}$$

where the matrices $[N_x], [B_x], [N_z]$, and $[B_z]$ contain the shape functions, their derivatives and the Jacobian components. The number of dofs of the problems in Ω_x and Ω_z domain are

$$Ndof_x = 2 \; n_x \; (N_n - 1) + 1 \tag{51}$$

$$Ndof_z = 2 \; n_z \; (N_n - 1) + 1 \tag{52}$$

where n_x and n_z are the total number of elements in $\Omega_x = \cup_{e=1}^{n_x}\Omega_x^e$ and $\Omega_z = \cup_{k=1}^{n_z}\Omega_z^k$ domain, respectively, and N_n is the number of nodes per element (can be different for each domain). For the load frequency, a uniform discretization of the interval $[\omega_{\min}, \omega_{\max}]$ is considered. The trapezoidal rule is used for the approximation of the integrals in α_ω, γ_ω, and β_ω. The size of vector g is denoted as n_ω and it coincides with the dofs of the problem in the load frequency domain.

4.1. Approximation on load frequency domain ω

Taking into account the discretization expressed by Equation (50), for each value of $\omega_j, j = 1, \ldots, n_\omega$, the variational Equation (26) can be rewritten as

$$g(\omega_j) = \frac{f_\omega + \omega_j^2 R_{\omega,M} - R_{\omega,K}}{k_\omega - \omega_j^2 m_\omega} \tag{53}$$

where

$$k_\omega = \sum_{e=1}^{nx} \int_{\Omega_x^e} \left[\tilde{\mathcal{E}}_v^e\right]^\top \left[\sum_{k=1}^{nz} \int_{\Omega_z^k} \left[\Sigma_z\left(\tilde{f}_k\right)\right]^\top \; [C_k] \; \left[\Sigma_z\left(\tilde{f}_k\right)\right] \; \mathrm{d}z\right] \; \left[\tilde{\mathcal{E}}_v^e\right] \; \mathrm{d}x \tag{54}$$

$$m_\omega = \sum_{e=1}^{nx} \int_{\Omega_x^e} [\tilde{v}_e]^\top \left[\sum_{k=1}^{nz} \int_{\Omega_z^k} \left[\tilde{F}_k\right]^\top \; \rho \; \left[\tilde{F}_k\right] \; \mathrm{d}z\right] \; [\tilde{v}_e] \; \mathrm{d}x \tag{55}$$

$$f_\omega = \left[\tilde{v}_{e_p}\right]^\top \; \left[\tilde{F}_{k_p}\right]^\top \; [f_d], \tag{56}$$

$$\begin{aligned} R_{\omega,M} &= \sum_{i=1}^{n-1} \bar{g}^i(\omega_j) \; \mu_\omega^i\left(\tilde{f}_k, \tilde{v}_e, \bar{u}\right); \\ R_{\omega,K} &= \sum_{i=1}^{n-1} \bar{g}^i(\omega_j) \; \sigma_\omega^i\left(\tilde{f}_k, \tilde{v}_e, \bar{u}\right) \end{aligned} \tag{57}$$

for e_p and k_p the elements where the load is applied.

4.2. Finite element approximation on Ω_z

The introduction of Equation (50) into the variational Equation (35) leads to the following linear system

$$([K_f] - [M_f])\left[q^f\right] = [F_f] - [R_f] \tag{58}$$

where $[q^f]$ is the vector of the nodal displacements associated with the finite element mesh in Ω_z, $[K_f]$ and $[M_f]$ are the stiffness and mass matrices obtained by assembling the element stiffness and mass matrices $[K_f^k]$ and $[M_f^k]$ respectively, $[F_f]$ is the load vector obtained by assembling the element load vectors $[F_f^k]$ and $[R_f]$ is the equilibrium residual obtained by assembling the element residual vectors $[R_f^k]$ whose expressions are

$$\left[K_f^k\right] = \gamma_\omega \int_{\Omega_z^k} [B_z]^\top \; \left[\sum_{e=1}^{n_x} [k_x(\tilde{v}_e)]\right] \; [B_z] \; \mathrm{d}z \tag{59}$$

$$\left[M_f^k\right] = \alpha_\omega \int_{\Omega_z^k} [N_z]^\top \; \left[\sum_{e=1}^{n_x} [m_x(\tilde{v}_e)]\right] \; [N_z] \; \mathrm{d}z \tag{60}$$

$$\left[F_f^k\right] = \beta_\omega \int_{\partial_F\Omega_z^k} [N_z]^\top \; \left[\sum_{e=1}^{n_x} [f_x(\tilde{v}_e)]\right] \; \mathrm{d}z \tag{61}$$

$$\begin{aligned} \left[R_f^k\right] = &\sum_{i=1}^{n-1} \gamma_\omega^i \int_{\Omega_z^k} [B_z]^\top \left[\sum_{e=1}^{n_x} \left[\sigma_x^i(\tilde{v}_e, \bar{u})\right]\right] \; \mathrm{d}z \\ &- \sum_{i=1}^{n-1} \alpha_\omega^i \int_{\Omega_z^k} [N_z]^\top \left[\sum_{e=1}^{n_x} \left[\mu_x^i(\tilde{v}_e, \bar{u})\right]\right] \; \mathrm{d}z \end{aligned} \tag{62}$$

4.3. Finite element approximation on Ω_x

Likewise, the introduction of Equation (50) into the variational Equation (44) leads to the linear system

Table 2. Vibration modes identified for different values of enrichment steps (1 = identified mode and 0 = non-identified mode).

Mode	PGD					ANSYS	Error (%)
	$N=5$	$N=10$	$N=20$	$N=30$	Ω	Ω	
bend	0	0	1	1	2.682	2.684	0.1
bend	0	0	1	1	9.336	9.346	0.1
t/c	1	1	1	1	15.684	15.685	0.0
bend	0	1	1	1	17.902	17.930	0.2
bend	1	0	1	1	27.249	27.307	0.2
th	0	1	1	1	31.198	31.203	0.0
bend	1	1	1	1	36.888	36.990	0.3
th	0	0	0	1	46.189	46.212	0.0
bend	0	0	1	1	46.609	46.771	0.3
sh	0	1	1	1	48.710	48.758	0.1

$$([K_v]-[M_v])[q^v]=[F_v]-[R_v] \tag{63}$$

where $[q^v]$ is the vector of the nodal displacements associated with the finite element mesh in Ω_x, $[K_v]$ and $[M_v]$ are the stiffness and mass matrices obtained by assembling the element stiffness and mass matrices $[K_v^e]$ and $[M_v^e]$ respectively, $[F_v]$ is the load vector obtained by assembling the element load vectors $[F_v^e]$ and $[R_v]$ is the equilibrium residual obtained by assembling the element residual vectors $[R_v^e]$ whose expressions are

$$\left[K_v^e\right]=\gamma_\omega\int_{\Omega_x^e}[B_x]^\top\left[\sum_{k=1}^{n_z}\left[k_z\left(\tilde{f}_k\right)\right]\right][B_x]\,\mathrm{d}x \tag{64}$$

$$\left[M_v^e\right]=\alpha_\omega\int_{\Omega_x^e}[N_x]^\top\left[\sum_{k=1}^{n_z}\left[m_z\left(\tilde{f}_k\right)\right]\right][N_x]\,\mathrm{d}x \tag{65}$$

$$\left[F_v^e\right]=\beta_\omega\int_{\partial_F\Omega_x^e}[N_x]^\top\left[\sum_{k=1}^{n_z}\left[f_z\left(\tilde{f}_k\right)\right]\right]\mathrm{d}x \tag{66}$$

$$\begin{aligned}\left[R_v^e\right]=&\sum_{i=1}^{n-1}\gamma_\omega^i\int_{\Omega_x^e}[B_x]^\top\left[\sum_{k=1}^{n_z}\left[\sigma_z^i\left(\tilde{f}_k,\bar{u}\right)\right]\right]\mathrm{d}x\\&-\sum_{i=1}^{n-1}\alpha_\omega^i\int_{\Omega_x^e}[N_x]^\top\left[\sum_{k=1}^{n_z}\left[\mu_z^i\left(\tilde{f}_k,\bar{u}\right)\right]\right]\mathrm{d}x\end{aligned} \tag{67}$$

4.4. Solution over the number of enrichment steps

Finally, the problem for the whole beam using a discrete PGD framework can be expressed by the three following equations

$$g(\omega_j)=\frac{f_\omega+\omega_j^2R_{\omega,M}-R_{\omega,K}}{k_\omega-\omega_j^2m_\omega},\quad\forall\quad j\in\{1,n_\omega\} \tag{68}$$

$$([K_f]-[M_f])\left[q^f\right]=[F_f]-[R_f] \tag{69}$$

$$([K_v]-[M_v])[q^v]=[F_v]-[R_v] \tag{70}$$

which are equivalent to Equations (21–23). This problem needs to be solved for each enrichment step $i=1,2,\ldots,n,\ldots,N$ following a fixed point iteration scheme. At the first step of the fixed point method, vectors g and q^f are initialized and q^v is computed using Equation (70). A key issue for the identification of different vibration modes is the initialization of the former vector, g. In this development, a different initialization is considered for each enrichment step n in the following manner

$$g^{(0)}(\omega_j)=\begin{cases}0 & j\neq i\\ 1 & j=i\end{cases}\text{ with }\ i=\arg\min_j|\omega_j-\Psi| \tag{71}$$

and Ψ is defined as

$$\Psi=\omega_{\min}+(n-1)\ \psi;\quad\psi=\frac{\omega_{\max}-\omega_{\min}}{N-1}$$

where N is the total number of enrichment steps and $[\omega_{\min},\omega_{\max}]$ is the considered load frequency range.

Regarding the initialization of q^f, a unity vector of size n_z is set for each enrichment step. After the computation of the vector q_v, the following steps of the fixed point algorithm are started by solving Equations (68–70) successively. The computation is iterated m times until the following convergence criteria are satisfied simultaneously

$$|\omega_n^{(m)}-\omega_n^{(m-1)}|<\varepsilon_\omega \tag{72}$$

$$\max\left\{\frac{\|\left(q^f\right)^{(m)}-\left(q^f\right)^{(m-1)}\|_2}{\|\left(q^f\right)^{(m-1)}\|_2},\frac{\|\left(q^v\right)^{(m)}-\left(q^v\right)^{(m-1)}\|_2}{\|\left(q^v\right)^{(m-1)}\|_2}\right\}<\varepsilon \tag{73}$$

being $\|\square\|_2$ the Euclidean norm and ε_ω and ε two different user-specified tolerances set to 10^{-2} and 10^{-6} in the following.

In this study, it has been noticed that the convergence at each enrichment step is not assured. It depends heavily on the number of vibration modes that the beam has in the studied load frequency range. Generally, a number of enrichment steps greater than the vibration modes present in the interval is needed. This means that some of the steps does not converge to a vibration mode. However, the information provided by this non-converging modes is important to reproduce the behavior of the beam in terms of the anti-resonant peaks. For the converging modes, about 15 iterations of the fixed point method have been required, at worst. For the non-converging modes, the maximum number of iterations is reached, which is set to 25 in this study. At each iteration, one equation with n_ω unknowns and two linear systems of dimension $Ndof_x$ and $Ndof_z$ are solved. In a classical layerwise FE approach, the performance implies n_ω resolutions with $\frac{Ndof_x\ \times\ Ndof_z}{2}$ dofs.

5. Numerical results

This section is dedicated to the analysis of some laminated and sandwich beams in order to evaluate the proposed approach in sections above. It should be noticed that the PGD method has been successfully used to solve static problems [47] of composite beams. This paper focuses on the harmonic analysis in the frequency domain, and the frequency response functions (FRF) are first obtained by using the PGD method. Moreover, the proposed formulation also

allows us to identify the modal parameters, natural frequencies and vibration modes.

Five different numerical test are analyzed below. A great variety of boundary conditions is considered with wide range of slenderness ratios for symmetric, anti-symmetric composite beams and different types of sandwich beams. In the following test, as far as the spatial discretization is concerned, a classical quadratic finite element approximation is considered for both domains Ω_x and Ω_z. A Gaussian numerical integration with three points is used to evaluate the elementary matrices and also to solve the integrals in load frequency domain. The results are compared with classical finite element solutions and exact elastic solutions or theories available in open literature. The commercial software ANSYS is employed in FE simulations to provide reference solutions. A bi-dimensional approach using the PLANE182 element with plane stress conditions is used. This element is defined by four nodes having two degrees of freedom at each node.

5.1. Convergence study of the PGD algorithm

A convergence study with respect to the number of total enrichment steps is first carried out. Then, the effect of the mesh size on both spatial coordinates and the load position are analyzed. For this purpose, a simple case of an isotropic beam is considered:

- *Geometry*: isotropic beam with $L = 10$ m and $h = 2$ m.
- *Material properties*: E=70 GPa, ν=0.3 and ρ=2,700 kg/m^3.
- *Boundary conditions*: simply supported beam submitted to a harmonic concentrated load.
- *Reference solution*: A modal analysis with a 2D FE model is performed using ANSYS. A refined regular mesh with square elements of side $L/100$ is considered.

5.1.1. Number of total enrichment steps

The convergence study with respect to the number of total enrichment steps N is first developed. The ten first modes are analyzed. In Table 2, the mode shapes are denoted as *bend*, *sh*, *t/c* and *th* for bending, shear, extensional and thickness modes, respectively. The natural frequencies are presented under a dimensionless value computed as $\Omega = \omega_n L S\sqrt{\rho/E}$. For PGD computations, a mesh of 50 elements on Ω_x domain and 10 elements on Ω_z is considered. The frequency search range is set to (40–800) Hz and the resolution to 1 Hz. The harmonic point load is applied at the top of the beam at a distance of $L/10$ from the support, and it has vertical and horizontal components with the same amplitude at each direction.

The study confirms that when looking for modes within a relatively wide frequency range, it is necessary to consider a number of steps greater than the number of vibration modes within that interval to effectively cover the entire frequency range. In this case, when twenty steps are considered, the algorithm manages to find nine of the ten modes present in that frequency range. When the number of steps is increased to thirty, the ten modes are identified. The relative errors made in the value of the natural frequency are kept below 0.3%.

Table 3. Relative error and cumulative error (in percentage) for the first four natural frequencies.

S_x \ S_z	h	$h/5$	$h/10$	$h/20$	Mode
	0.586	0.010	0.009	0.010	1
	1.719	0.054	0.051	0.050	2
$L/10$	0.009	0.001	0.001	0.001	3
	2.805	0.166	0.160	0.160	4
	5.12	**0.23**	**0.22**	**0.22**	cum.
	0.578	0.002	0.001	0.001	1
	1.671	0.006	0.003	0.003	2
$L/20$	0.002	0.000	0.000	0.000	3
	2.654	0.017	0.011	0.010	4
	4.90	**0.02**	**0.02**	**0.01**	cum.
	0.577	0.001	0.000	0.000	1
	1.668	0.003	0.000	0.000	2
$L/50$	0.002	0.000	0.000	0.000	3
	2.643	0.007	0.001	0.000	4
	4.89	**0.01**	**0.00**	**0.00**	cum.
	0.577	0.001	0.001	ref.	1
	1.668	0.003	0.000	ref.	2
$L/100$	0.002	0.000	0.000	ref.	3
	2.643	0.007	0.000	ref.	4
	4.89	**0.01**	**0.00**	–	cum.

5.1.2. Spatial domain mesh

The convergence study with regard to the spatial domain mesh is carried out in this section. In the analysis, the frequency search range is reduced to (40–450) Hz because only the results for the first four modes are compared. In this case, it is enough to consider $N = 10$ enrichment steps. The frequency resolution is 1 Hz and a concentrated harmonic load is applied at the top of the beam at a distance of $L/10$ from the support, with vertical and horizontal components, as for the previous section. Table 3 shows the relative and cumulative errors of the first four natural frequencies for different meshes. Errors are calculated for the finest mesh considered as reference. Parameters S_x and S_z represent the relative mesh size in beam and thickness axis respectively.

It can be inferred from Table 3 that the convergence rate is rather high and a mesh with n_x=20 (S_x=$L/20$) and n_z=5 (S_z=$h/5$) elements is sufficient to obtain converged results.

5.1.3. Load position

The influence of the position and direction of the load applied is evaluated herein. Horizontal and vertical concentrated harmonic loads are considered separately, as well as different load application points. The converged PGD spatial mesh is used following Table 3. The frequency range and number of enrichment steps are the same as in Section 5.1.2. In Figure 2, a simplified representation of the first five mode shapes of the isotropic beam are plotted with dashed line. Table 4 shows which of these five modes are identified when changing the direction and position of the load.

The results report that when a vertical load is placed in the center of the beam ($L/2$) the modes b and e are not excited. This is because for these modes the middle section of the beam, where the load is applied, does not move vertically. Analogously, when a horizontal load is placed in the

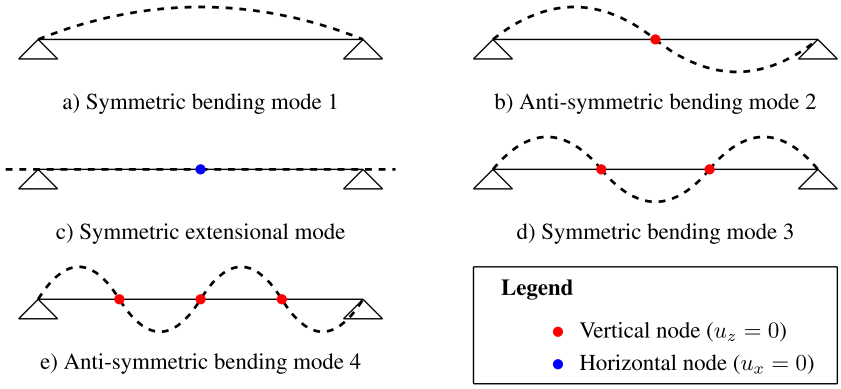

Figure 2. First five modal shapes of the isotropic beam with S = 5.

middle of the beam, mode c cannot be identified because that section does not move horizontally. In view of these results, to ensure the identification of all modes, a load with both vertical and horizontal components should be considered and not located in a node. Hereafter, a concentrated load with both components located at a distance of $L/10$ from the beam support is considered in the following tests.

5.2. Symmetric and anti-symmetric laminated beam

In this section, two symmetric and anti-symmetric composite cross-ply beams analyzed in reference [48] are considered. The aim of this analysis is to asses the performance of the proposed method to model laminated beams with different length to thickness ratios. The characteristics of the test are described as follows:

- *Geometry*: $(0^\circ/90^\circ/0^\circ)$ with thickness $0.25h/0.25h/0.25h$; $(0°/90°)$, being the two layers the same thickness; four length to thickness ratios $S = 2$, 5, 10, and 20.
- *Material properties*: $E_L = 181$ GPa, $E_T = 10.3$ GPa, $G_{LT} = 7.17$ GPa, $G_{TT} = 2.87$ GPa, $\nu_{LT} = 0.25$, $\nu_{TT} = 0.33$ and $\rho = 1578$ kg/m^3. Subscripts L and T refer to the fiber and transverse direction respectively.
- *Boundary conditions*: simply supported beam with a harmonic concentrated load placed on the top layer at a distance of $L/10$ from the first support.

The results are presented in a dimensionless form. The dimenssionless natural frequency is computed as $\Omega = \omega_n L S\sqrt{\rho/E_T}$. The numerical values obtained with the PGD method are compared with exact two-dimensional elasticity solution from [48] and results computed with the commercial software ANSYS using a very refined mesh. For further information about the calculation parameters, please refer to the Appendix A. Table 5 presents the values of the first seven natural frequencies for the thin to very thick of both symmetric and anti-symmetric beams. These results show the excellent agreement with reference values for all types of modes. The maximum relative error is below 0.86%. Figures 3 and 4 represent the first six vibration modes for the very thick beams. The PGD algorithm is able to detect not only bending modes, but also shear and thickness modes with complex displacement distribution along either the beam axis or the thickness.

Table 4. Vibration modes identified for different load positions (1 = identified mode and 0 = non-identified mode).

Mode	Vertical load			Horizontal load		
	$L/10$	$L/4$	$L/2$	$L/10$	$L/4$	$L/2$
a	1	1	1	0	0	0
b	1	1	0	0	0	0
c	0	0	1	1	1	0
d	1	1	1	0	0	0
e	1	0	0	0	0	0

The main goal of this research is to solve the dynamic problem of a forced vibration beam subjected to a general harmonic excitation of frequency ω (Equation (13)). Damping is not considered in the formulation and the displacements are theoretically infinite for loads with a frequency equal to the resonance frequencies of the structure. The frequency response of a system can be represented in terms of displacement, velocity or acceleration considering different graphical representation: real and imaginary parts again frequency, Bode diagrams or Nyquist plot. Herein, the bode representation of displacement-force relationship, so-called receptance, is considered. In Figure 5 the FRF of vertical and horizontal displacements at the load application point are plotted for the symmetric laminated beam with $S = 5$. The first seven natural frequencies that appear in Table 5 can be distinguished in this graphical representation.

In Figure 6 a detail of the horizontal displacement FRF (Figure 5a) in the range of $\Omega = [43-45]$ is presented. It can be observed that both extensional mode ($\Omega = 43.649$) and shear mode ($\Omega = 43.793$) have been identified despite having very similar natural frequency values.

Using the linear scale in magnitude-frequency graphs lead to lose detail of the response. In order to avoid this, plots are usually presented using logarithmic scales or, at least, vertical logarithmic scale. Bode plots of the receptance amplitude in dB is depicted in the following. The value of the receptance α in dB is defined as:

$$\alpha(\mathrm{dB}) = 20\log_{10}\left(\frac{\alpha}{\alpha_{ref}}\right) \tag{74}$$

where α_{ref} is a reference value, assumed as unity in this study. Figure 7 shows the good agreement between the

Table 5. Dimensionless natural frequencies of the symmetric and anti-symmetric laminated beams.

	Symmetric lay-up					Anti-symmetric lay-up			
S	Mode	Exact 2D [48]	ANSYS	PGD	Error (%)	Mode	ANSYS	PGD	Error (%)
2	*bend*	–	3.447	3.447	0.0	*bend*	3.206	3.205	0.0
	sh	–	7.007	7.007	0.0	*bend*	7.406	7.404	0.0
	bend	–	7.689	7.686	0.0	*sh*	7.762	7.761	0.0
	th	–	10.788	10.786	0.0	*th*	8.818	8.817	0.0
	bend	–	12.015	12.009	0.1	*bend*	10.987	10.982	0.0
	th	–	12.808	12.803	0.0	*th*	12.835	12.833	0.0
	th	–	14.966	14.963	0.0	*th*	13.465	13.462	0.0
5	*bend*	6.806	6.808	6.806	0.0	*bend*	4.782	4.779	0.0
	bend	16.515	16.524	16.514	0.1	*bend*	14.653	14.638	0.1
	bend	26.688	26.718	26.688	0.1	*bend*	25.496	25.461	0.1
	bend	37.255	37.323	37.256	0.2	*th*	35.396	35.382	0.0
	t/c	–	43.672	43.649	0.1	*bend*	36.181	36.119	0.2
	sh	–	43.807	43.793	0.0	*bend*	46.367	46.273	0.2
10	*bend*	48.035	48.155	48.037	0.2	*sh*	48.536	48.505	0.0
	bend	9.343	9.347	9.343	0.0	*bend*	5.297	5.293	0.1
	bend	27.224	27.249	27.223	0.1	*bend*	19.150	19.117	0.2
	bend	46.416	46.485	46.417	0.1	*bend*	37.855	37.755	0.3
	bend	66.058	66.195	66.056	0.2	*bend*	58.759	58.553	0.4
	bend	86.169	86.420	86.168	0.3	*bend*	80.478	80.134	0.4
	t/c	–	93.776	93.738	0.0	*t/c*	88.435	88.395	0.0
20	*bend*	106.75	107.166	106.750	0.4	*bend*	102.350	101.842	0.5
	bend	10.64	10.649	10.640	0.1	*bend*	5.465	5.453	0.2
	bend	37.374	37.439	37.373	0.2	*bend*	21.234	21.171	0.3
	bend	71.744	71.939	71.743	0.3	*bend*	45.708	45.517	0.4
	bend	108.89	109.293	108.895	0.4	*bend*	76.903	76.473	0.6
	bend	147.04	147.712	147.039	0.5	*bend*	112.951	112.486	0.4
	bend	185.68	186.712	185.681	0.6	*bend*	152.336	151.031	0.9
	t/c	–	190.553	190.491	0.0	*t/c*	187.926	187.863	0.0

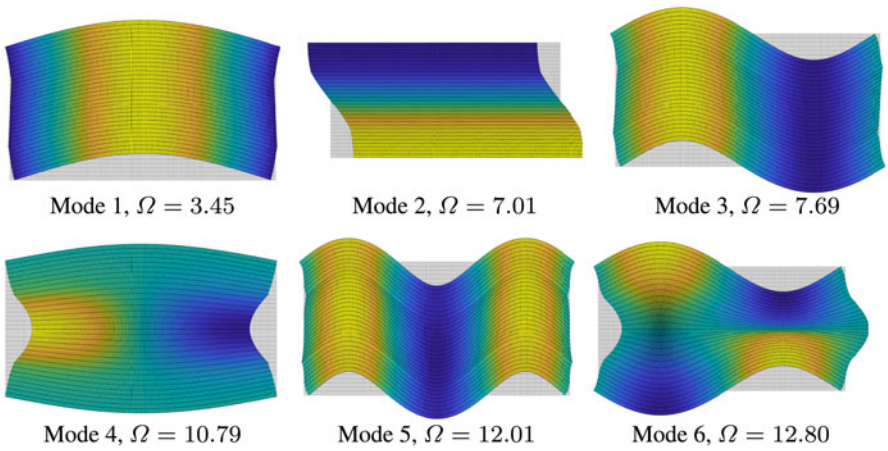

Figure 3. Proper generalized decomposition (PGD) solution of mode shapes for the symmetric laminated beam (0°/90°/0°) with $S = 2$.

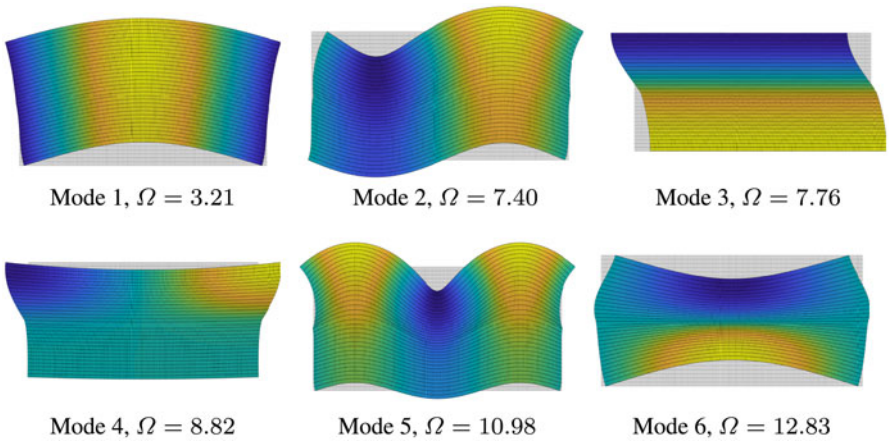

Figure 4. Proper generalized decomposition (PGD) solution of mode shapes for the anti-symmetric laminated beam (0°/90°) with $S = 2$.

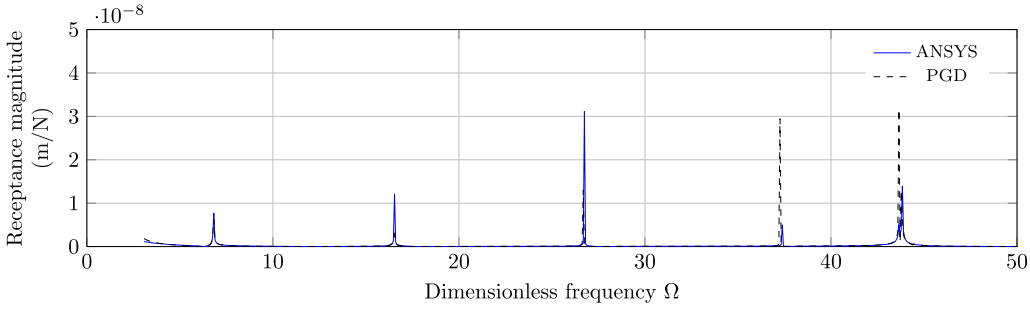

(a)

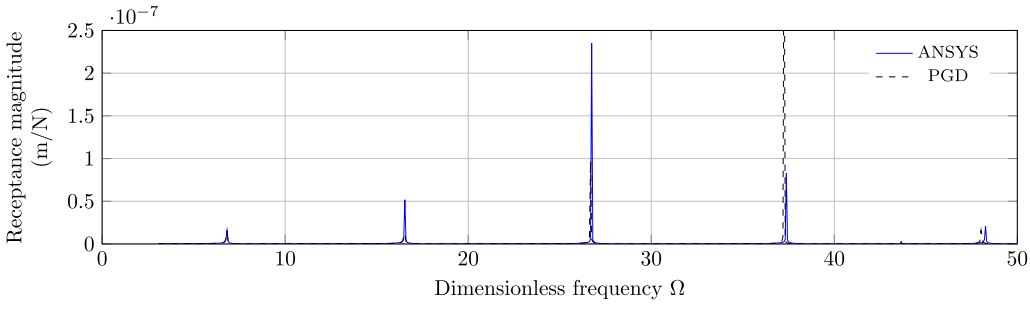

(b)

Figure 5. Frequency response functions (FRF) at load application point for the symmetric laminated beam (0°/90°/0°) with $S = 5$: (a) horizontal displacement, (b) vertical displacement.

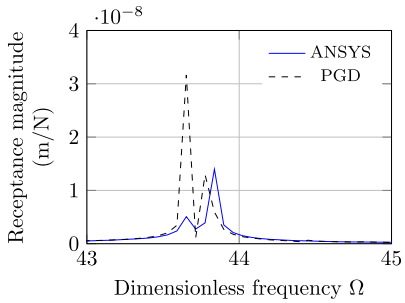

Figure 6. Detail of the horizontal displacement frequency response functions (FRF) for the symmetric laminated beam (0°/90°/0°) with $S = 5$.

amplitude of horizontal and vertical displacements at middle point of the beam calculated through a harmonic analysis in ANSYS and using the proposed PGD formulation. The most important difference between this representation in semi-logarithmic scale and the previous one is that the anti-resonance peaks can be detected. This particular feature of the direct point receptance can be used to evaluate the validity of the computed FRF using the PGD method.

5.3. Three-layer sandwich beam

In order to evaluate the PGD algorithm for solving problems in composite beams with layers of very different characteristics, the present test consists of a three-layer sandwich beam composed of two graphite-epoxy faces and a soft core with the following properties [48]:

- *Geometry*: Three layers of thickness $0.1h/0.8h/0.1h$ and four length to thickness ratios $S = 2$, 5, 10, and 20.
- *Material properties*:
  Face: $E_{1f} = 131.1$ GPa, $E_{2f} = E_{3f} = 6.9$ GPa, $G_{12f} = 3.588$ GPa, $G_{13f} = 3.088$ GPa, $G_{23f} = 2.3322$ GPa, $\nu_{12f} = \nu_{13f} = 0.32$, $\nu_{23f} = 0.49$ and $\rho_f = 1000$ kg/m^3.
  Core: $E_{1c} = 0.2208$ MPa, $E_{2c} = 0.2001$ MPa, $E_{3c} = 2760$ MPa, $G_{12c} = 16.56$ MPa, $G_{13c} = 545.1$ MPa, $G_{23c} = 455.4$ MPa, $\nu_{12c} = 0.99$, $\nu_{13c} = \nu_{23c} = 0.00003$ and $\rho_c = 70$ kg/m^3.
- *Boundary conditions*: simply supported beam with a harmonic concentrated load placed on the top layer at a distance of $L/10$ from the beam start.

The dimensionless natural frequency is computed as $\Omega = \omega_n LS\sqrt{(\rho_f/E_{2f})}$, where subscript f refers to the face material properties. The results are compared with exact 2D elasticity solution from [48] and results computed with ANSYS. The parameters used for the finite element model and for the PGD simulation are provided in the Appendix A. Table 6 presents the values of the first seven natural frequencies for the thin to very thick three-layer sandwich beam. It can be noticed that the natural frequencies given by the PGD method are in excellent agreement with the reference elasticity solution in [48] for all types of modes, including thickness modes. Errors with respect to the ANSYS solution remain below 0.5% for thin to thick beams ($S = 20$, 10, and 5) and only go up to 1% for the very thick case ($S = 2$). Note that the refined sinus model [49], denoted with SinRef-7p, which includes the transverse normal deformation and the zig-zag effect, fails to predict the thickness mode with accuracy. As in the present formulation, the use of layerwise approach is required.

Figure 8 represents the first three thickness modes for the very thick beam. As it can be observed, even

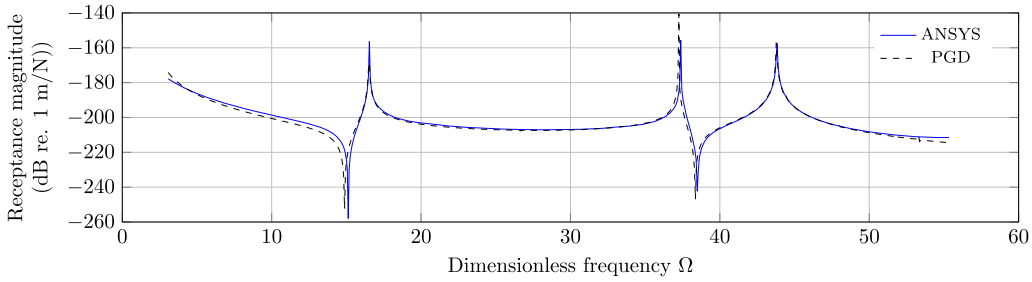

(a)

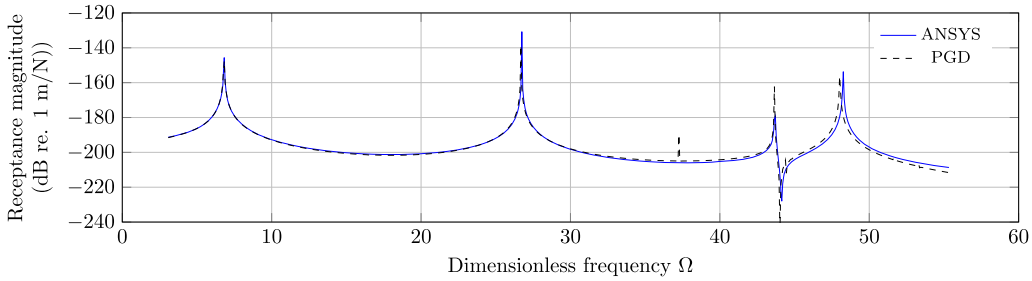

(b)

Figure 7. Frequency response functions (FRF) at bottom midpoint for the symmetric laminated beam (0°/90°/0°) with $S = 5$: (a) horizontal displacement and (b) vertical displacement.

Table 6. Dimensionless natural frequencies of the three layer sandwich beam.

S	Mode	Exact 2D [48]	ANSYS	PGD	Error (%)	SinRef-7p	Error (%)
2	*bend*	–	3.519	3.521	0.0	3.53	0.2
	sh	–	5.340	5.340	0.0	5.34	0.1
	bend	–	7.531	7.562	0.4	7.60	0.2
	th	–	11.599	11.627	0.2	11.07	4.0
	th	–	11.663	11.664	0.0	9.40	19.0
	bend	–	11.823	11.954	1.1	11.97	0.2
	th	–	12.036	12.161	1.0	15.00	24.0
5	*bend*	7.8227	7.817	7.815	0.0	7.83	0.1
	bend	17.274	17.253	17.247	0.0	17.31	0.1
	bend	26.903	26.854	26.847	0.0	26.97	0.2
	sh	–	33.377	33.372	0.0	33.37	0.1
	bend	36.937	36.838	36.844	0.0	37.06	0.1
	bend	47.397	47.223	47.265	0.1	47.58	0.1
	bend	58.221	57.944	58.052	0.2	–	–
10	*bend*	12.237	12.235	12.230	0.0	12.26	0.1
	bend	31.291	31.281	31.260	0.1	31.33	0.1
	bend	50.218	50.205	50.154	0.1	50.31	0.1
	bend	68.096	69.088	68.990	0.1	69.26	0.1
	bend	88.18	88.190	88.021	0.2	88.51	0.1
	bend	107.61	107.660	107.389	0.3	108.25	0.2
	t/c	–	120.032	120.018	0.0	121.11	0.9
20	*bend*	15.382	15.389	15.379	0.1	15.41	0.2
	bend	48.948	48.989	48.922	0.1	49.04	0.1
	bend	86.902	87.010	86.833	0.2	87.07	0.1
	bend	125.16	125.374	125.042	0.3	–	–
	bend	163.12	163.479	162.941	0.3	163.69	0.1
	bend	200.87	201.423	200.618	0.4	201.94	0.1
	bend	–	239.387	238.243	0.5	–	–

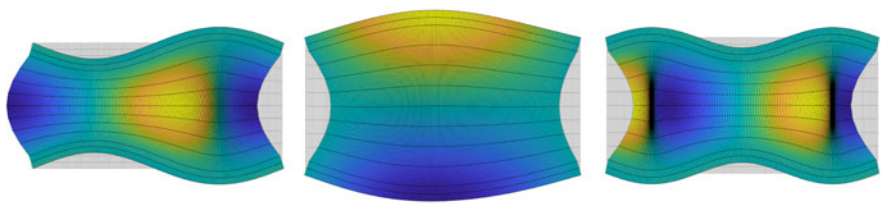

Mode 4, $\Omega = 11.63$ Mode 5, $\Omega = 11.66$ Mode 7, $\Omega = 12.16$

Figure 8. Proper generalized decomposition (PGD) solution of thickness modes for the three-layer sandwich beam with $S = 2$.

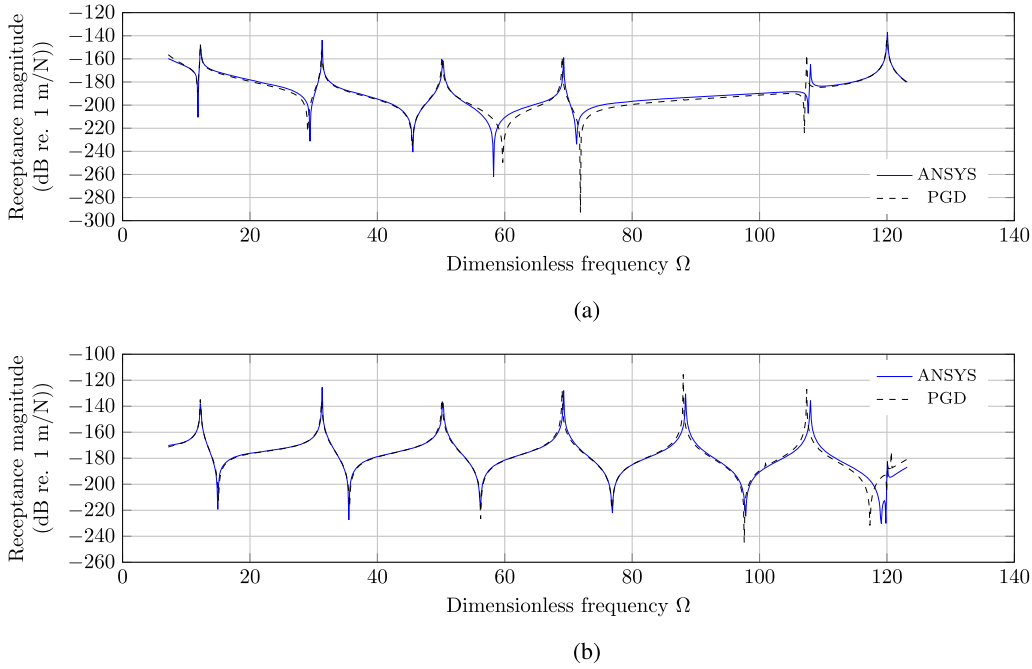

Figure 9. Frequency response functions (FRF) at load application point for the three-layer sandwich beam with $S = 10$: (a) horizontal displacement and (b) vertical displacement.

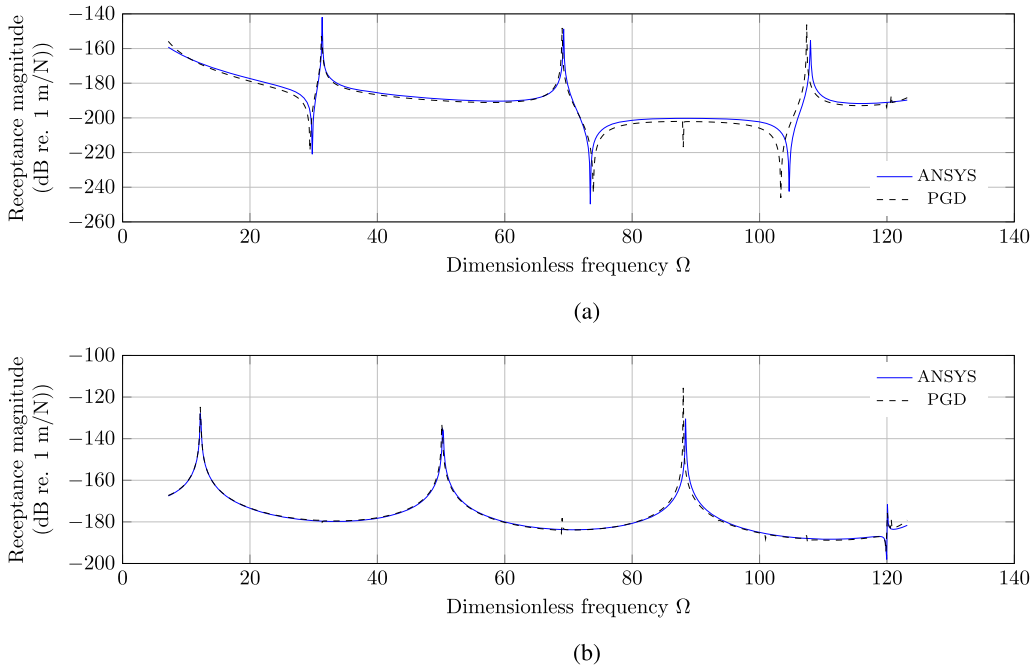

Figure 10. Frequency response functions (FRF) at bottom midpoint for the three-layer sandwich beam with $S = 10$: (a) horizontal displacement and (b) vertical displacement.

Table 7. Dimensionless natural frequencies of the unsymmetric sandwich beam.

		ANSYS	PGD		SinRef-7p		GLHT		ZZT	
S	Mode	Ω	Ω	Error (%)	Ω	Error (%)	Ω	Error (%)	Ω	Error (%)
4	*bend 1*	0.614	0.614	0.1	0.645	5.0	0.638	4.0	0.616	0.3
	bend 2	1.762	1.763	0.1	1.819	3.2	1.800	2.2	1.772	0.6
	bend 3	3.569	3.572	0.1	3.674	2.9	3.631	1.7	3.621	1.5
	bend 4	5.795	5.802	0.1	6.223	7.3	6.133	5.8	6.186	6.8
10	*bend 1*	1.282	1.283	0.1	1.361	6.1	1.347	5.0	1.282	0.0
	bend 2	2.868	2.870	0.1	3.026	5.5	2.994	4.4	2.875	0.2
	bend 3	4.951	4.954	0.1	5.183	4.6	5.126	3.5	4.971	0.4
	bend 4	7.649	7.653	0.0	7.961	4.0	7.861	2.7	7.686	0.4

Table 8. Fundamental dimensionless natural frequencies for different boundary conditions.

		FF	CC	SF	CS	SS	CF
ANSYS	Ω	19.097	10.757	13.465	9.825	9.200	4.153
PGD	Ω	19.225	10.816	13.875	10.056	9.199	4.218
	Error (%)	0.7	0.6	3.0	2.4	0.0	1.6
SinRef-7p	Ω	19.123	11.100	13.472	10.000	9.201	4.189
	Error (%)	0.1	3.2	0.1	1.8	0.0	0.9
$PSDBT_{cs}$	Ω	18.976	11.446	13.206	10.032	8.968	4.158
	Error (%)	0.6	6.4	1.9	2.1	2.5	0.1
$HSDBT_{cs}$	Ω	18.955	11.427	13.195	10.021	8.964	4.157
	Error (%)	0.7	6.2	2.0	2.0	2.6	0.1
$PSDBT_{ds}$	Ω	19.391	11.637	13.538	10.236	9.207	4.233
	Error (%)	1.5	8.2	0.5	4.2	0.1	1.9
$HSDBT_{ds}$	Ω	19.401	11.625	13.538	10.229	9.207	4.232
	Error (%)	1.6	8.1	0.5	4.1	0.1	1.9
Minimum error Model		**0.1** SinRef-7p	**0.6** PGD	**0.1** SinRef-7p	**1.8** SinRef-7p	**0.0** PGD	**0.1** $HSDBT_{cs}$

nonsymmetrical modes (cf. mode 4) can be obtained with PGD formulation.

Figures 9 and 10 represent the frequency response function of vertical and horizontal displacements separately, at the load application point and at the bottom midpoint of the beam, respectively. In these figures, only the response of the beam with a slenderness ratio of S = 10 is represented. In this case, the first six natural frequencies correspond to six bending modes, as it is remarked in Table 6. The differences between these two below figures are quite remarkable. In Figure 9, almost all natural frequencies can be identified in both vertical and horizontal displacement, but it is not the same in Figure 10. This is due to the fact that the vibration nodes of various bending modes are located at the central point of the beam. Regarding symmetrical vibration bending modes (odd modes), they do not have horizontal displacement but vertical displacement at bottom midpoint of the beam as it can be observed in Figure 10(b). Conversely, for the anti-symmetric bending modes (even modes) the opposite occurs, cf. Figure 10(a). The PGD results are in good concordance with ANSYS solution.

5.4. Unsymmetric sandwich beam

The aim of this section is to compare the results of the PGD method with other theories available in the literature. For this purpose, a sandwich beam analyzed in the reference [50] is chosen as a test. This is an unsymmetric sandwich beam composed of two laminated faces with a core between them. Each face is composed of two layers with an orthogonal orientation stacking sequence: $0^\circ/90^\circ/\text{core}/0^\circ/90^\circ$.

- *Geometry*: Five layers of thickness $0.5h_f/0.5h_f/\ h_c/\ 0.5h_f/0.5h_f$ with $h_c/h_f = 10$ and two length to thickness ratios $S = 4$ and 10.
- *Material properties*:
  Face laminated: $E_{1f} = 131.1$ GPa, $E_{2f} = E_{3f} = 10.34$ GPa, $G_{12f} = G_{23f} = 6.895$ GPa, $G_{13f} = 6.205$ GPa, $\nu_{12f} = \nu_{13f} = 0.22$, $\nu_{23f} = 0.49$ and $\rho_f = 1627\ \text{kg/m}^3$.
  Isotropic core: $E_c = 6.89$ MPa, $G_c = 3.45$ MPa, $\nu_c = 0$ and $\rho_c = 97\ \text{kg/m}^3$.
- *Boundary conditions*: simply supported beam with a vertical harmonic load placed on the top layer at a distance of $L/10$ from the beam start.

Table 7 presents the values of the first four bending frequencies for the thick and semi-thick unsymmetric sandwich beam. The frequencies are displayed in dimensionless form as in Section 5.3. The results obtained with the PGD method are compared with those obtained applying three models reported from [49, 50] denoted as:

- GLHT: global-local-higher order theory [51].
- ZZT: zig-zag theory satisfying the continuity of transverse shear stress at interfaces [18].
- SinRef-7p: refined sinus model satisfying the continuity of transverse shear stress at interfaces with seven independent generalized displacements [49].

A 2D finite element model of the unsymmetric sandwich beam has also been developed and used as reference for the comparison of the results of the different models (see ANSYS and PGD calculation parameter details in the Appendix A). It can be noticed that the natural frequencies obtained with the PGD method are in excellent agreement with the reference solution for both thick and semi-thick beams. The error rate is less than 0.12%. This example highlights the limitations of high-order ESL models for such structures, especially for the thick case. In contrast, the present layer-wise approach based on the variable separation is well-adapted.

5.5. Influence of boundary conditions

Lastly, to validate the PGD algorithm for different boundary conditions, a symmetric laminated composite beam with an orientation stacking sequence $0^\circ/90^\circ/0^\circ$ with the following characteristics is analyzed:

- *Geometry*: Three layers of equal thickness and a length to thickness ratio $S = 5$.
- *Material properties*: $E_L/E_T = 40, G_{LT} = 0.2 \cdot E_T, G_{TT} = 0.5 \cdot E_T, \nu_{LT} = 0.25, \nu_{TT} = 0.33$ and $\rho = 1\ \text{kg/m}^3$.
- *Boundary conditions*: beam with a harmonic concentrated load placed on the top layer at a distance of $L/10$ from the beam start. Six different support cases: free/free (FF), clamped/clamped (CC), simply support/free (SF), clamped/simply support (CS), simply support/simply support (SS), and clamped/free (CF).

The PGD solution is compared with the results of SinRef-7p model from [49] and with those calculated in [52] using theories named as:

- $PSDBT_{cs/ds}$: parabolic shear deformation beam theory with continuous/discontinuous inter-laminar stresses.
- $HSDBT_{cs/ds}$: Hyperbolic shear deformation beam theory with continuous/discontinuous inter-laminar stresses.

As in the previous section, a finite element model of the symmetric laminated beam with the different boundary conditions is analyzed. A unity value of parameter E_T is set for the analysis. The rest of the parameters of the finite element model and those referring to the resolution using the PGD method can be found in Appendix A.

Table 8 shows the fundamental natural frequencies expressed in dimensionless form as in Section 5.2 for the PGD approximation and for the five previous models. As a general remark, the highest frequencies occur for the free/free boundary condition and the lowest values is obtained for the cantilever beam (clamped/free case). For the models with continuous inter-laminar stresses (including the SinRef-7p model), the frequencies for the PGD model are always higher than those of the two other models, except for the CC condition. Concerning the models with discontinuous inter-laminar stresses, the PGD results are always lower than the two other discontinuous models, except for the SF condition. The differences between PGD solution and those obtained with the other models remain always low. With respect to the ANSYS solution for a very refined mesh of 3,375 elements, the PGD method solution is the best fit for SS and CC cases. For the other boundary conditions, PGD errors do not exceed 3%.

6. Conclusions

This paper investigates a new methodology based on the PGD method to solve the forced vibration problem in bi-dimensional laminated beams. A classical harmonic space-frequency description of the dynamic problem is considered and a variable separation in the spatial domain is introduced. For both spatial coordinates x (beam axis coordinate) and z (thickness coordinate), a classical 3-node FE is used in the discretization while a linear interpolation is introduced for the load frequency ω. The derived iterative algorithm implies the computation of three 1D functions at each iteration where the total cost depends on the number of enrichment steps N used to represent the solution. Specifically the proposed process requires, for each enrichment step, a small number of iterations m of the fixed point method which involves the resolution of one equation with n_ω unknowns and two linear systems of $Ndof_x$ and $Ndof_z$ dofs respectively. In a classical layerwise FE approach, the calculation implies n_ω resolutions with $\frac{Ndof_x \times Ndof_z}{2}$ dofs. The advantages of the proposed algorithm become relevant when the number of numerical layers and the number of elements in axis direction increases.

The new approach has been used to solve numerical tests, including different composite and sandwich beam configurations with a great variety of slenderness ratios and boundary conditions. Results show a good agreement with exact elasticity solutions, higher-order theories and FE models. This study has showed the interesting capability of the method to build all kinds of mode shapes, including complex thickness modes with non-uniform displacement distribution along x and z axis. This is possible owing to the present layerwise approach.

ORCID

María Infantes http://orcid.org/0000-0002-3024-7894

References

[1] Y. Tanigawa, H. Murakami, and Y. Ootao, Transient thermal stress analysis of a laminated composite beam, J. Thermal Stresses, vol. 12, no. 1, pp. 25–39, 1989. DOI: 10.1080/01495738908961952.

[2] S. M. Nabi and N. Ganesan, A generalized element for the free vibration analysis of composite beams, Compos. Struct., vol. 51, no. 5, pp. 607–610, 1994. DOI: 10.1016/0045-7949(94)90068-X.

[3] Y. Teboub and P. Hajela, Free vibration of generally layered composite beams using symbolic computations, Compos. Struct., vol. 33, no. 3, pp. 123–134, 1995. DOI: 10.1016/0263-8223(95)00112-3.

[4] V. Yildirim, Effect of the longitudinal to transverse moduli ratio on the in-plane natural frequencies of symmetric cross-ply laminated beams by the stiffness method, Compos. Struct., vol. 50, pp. 319–326, 2000.

[5] A. Chakraborty, R. Roy Mahapatra, and S. Gopalakrishnan, Finite element analysis of free vibration and wave propagation in asymmetric composite beams with structural discontinuities, Compos. Struct., vol. 55, no. 1, pp. 23–36, 2002. DOI: 10.1016/S0263-8223(01)00130-1.

[6] V. K. Goyal, and R. K. Kapania, A shear-deformable beam element for the analysis of laminated composites, Finite Elem. Anal. Des., vol. 43, no. 6–7, pp. 463–477, 2007. DOI: 10.1016/j.finel.2006.11.011.

[7] L. Jun, H. Hongxing, and S. Rongying, Dynamic finite element method for generally laminated composite beams, Int. J. Mech. Sci., vol. 50, no. 3, pp. 466–480, 2008. DOI: 10.1016/j.ijmecsci.2007.09.014.

[8] K. Chandrashekhara and K. M. Bangera, Free vibration of composite beams using a refined shear flexible beam element, Comput. Struct., vol. 43, no. 4, pp. 719–727, 1992. DOI: 10.1016/0045-7949(92)90514-Z.

[9] G. Shi and K. Y. Lam, Finite element vibration analysis of composite beams based on higher-order beam theory, J. Sound Vibr., vol. 219, no. 4, pp. 707–721, 1999. DOI: 10.1006/jsvi.1998.1903.

[10] H. Matsunaga, Vibration and buckling of multilayered composite beams according to higher order deformation theories, J. Sound Vibr., vol. 246, no. 1, pp. 47–62, 2001. DOI: 10.1006/jsvi.2000.3627.

[11] M. V. V. S. Murthy, D. Roy Mahapatra, K. Badarinarayana, and S. Gopalakrishnan, A refined higher order finite element for asymmetric composite beams, Compos. Struct., vol. 67, no. 1, pp. 27–35, 2005. DOI: 10.1016/j.compstruct.2004.01.005.

[12] T. Kant, S. R. Marur, and G. S. Rao, Analytical solution to the dynamic analysis of laminated beams using higher order refined theory, Compos. Struct., vol. 40, no. 1, pp. 1–9, 1997. DOI: 10.1016/S0263-8223(97)00133-5.

[13] M. K. Rao, Y. M. Desai, and M. R. Chitnis, Free vibrations of laminated beams using mixed theory, Comput. Struct., vol. 52, pp. 149–160, 2001. DOI: 10.1016/S0263-8223(00)00162-8.

[14] P. Subramanian, Dynamic analysis of laminated composite beams using higher order theories and finite elements, Compos. Struct., vol. 73, no. 3, pp. 342–353, 2006. DOI: 10.1016/j.compstruct.2005.02.002.

[15] R. P. Shimpi and A. V. Ainapure, A beam finite element based on layerwise trigonometric shear deformation theory, Compos. Struct., vol. 53, no. 2, pp. 153–162, 2001. DOI: 10.1016/S0263-8223(00)00186-0.

[16] M. Tahani, Analysis of laminated composite beams using layerwise displacement theories, Compos. Struct., vol. 79, no. 4, pp. 535–547, 2007. DOI: 10.1016/j.compstruct.2006.02.019.

[17] W. Zhen and C. Wanji, An assessment of several displacement-based theories for the vibration and stability analysis of laminated composite and sandwich beams, Compos. Struct., vol. 84, no. 4, pp. 337–349, 2008. DOI: 10.1016/j.compstruct.2007.10.005.
[18] M. Cho and R. Parmerter, Efficient higher-order composite plate theory for general lamination configurations, Aiaa J., vol. 31, pp. 1299–1306, 1993.
[19] R. C. Averill and Y. C. Yip, Thick beam theory and finite element model with zig-zag sublaminate approximations, Aiaa J., vol. 34, no. 8, pp. 1627–1632, 1996. DOI: 10.2514/3.13281.
[20] S. Kapuria, P. C. Dumir, and A. Ahmed, An efficient higher order zigzag theory for composite and sandwich beams subjected to thermal loading, Int. J. Solids Struct., vol. 40, no. 24, pp. 6613–6631, 2003. DOI: 10.1016/j.ijsolstr.2003.08.014.
[21] P. Vidal and O. Polit, A family of sinus finite elements for the analysis of rectangular laminated beams, Compos. Struct., vol. 84, no. 1, pp. 56–72, 2008. DOI: 10.1016/j.compstruct.2007.06.009.
[22] P. Vidal and O. Polit, A refined sine-based finite element with transverse normal deformation for the analysis of laminated beams under thermomechanical loads, JOMMS, vol. 4, no. 6, pp. 1127–1155, 2009. DOI: 10.2140/jomms.2009.4.1127.
[23] P. Vidal and O. Polit, A sine finite element using a zig-zag function for the analysis of laminated composite beams, Compos. B: Eng. J., vol. 42, no. 6, pp. 1671–1682, 2011. DOI: 10.1016/j.compositesb.2011.03.012.
[24] E. Carrera, Historical review of zig-zag theories for multilayered plates and shells, Appl. Mech. Rev., vol. 56, no. 3, pp. 287–308, 2003. DOI: 10.1115/1.1557614.
[25] E. Carrera, Evaluation of layerwise mixed theories for laminated plates analysis, Aiaa J., vol. 36, no. 5, pp. 830–839, 1998. DOI: 10.2514/2.444.
[26] E. Carrera and L. Demasi, Classical and advanced multilayered plate elements based upon PVD and RMVT. Part 1: Derivation of finite element matrices, Int. J. Num. Meth. Eng., vol. 55, no. 2, pp. 191–231, 2002. DOI: 10.1002/nme.492.
[27] E. Carrera and L. Demasi, Classical and advanced multilayered plate elements based upon PVD and RMVT. Part 2: Numerical implementations, Int. J. Num. Meth. Eng., vol. 55, no. 3, pp. 253–291, 2002. DOI: 10.1002/nme.493.
[28] A. K. Noor and W. S. Burton, Assessment of computational models for multilayered composite shells, Appl. Mech. Rev., vol. 43, no. 4, pp. 67–97, 1990. DOI: 10.1115/1.3119162.
[29] J. N. Reddy, Mechanics of Laminated Composite Plates – Theory and Analysis. CRC Press, Boca Raton, FL, 1997.
[30] E. Carrera, Theories and finite elements for multilayered, anisotropic, composite plates and shells, ARCO, vol. 9, no. 2, pp. 87–140, 2002. DOI: 10.1007/BF02736649.
[31] Y. X. Zhang and C. H. Yang, Recent developments in finite elements analysis for laminated composite plates, Compos. Struct., vol. 88, no. 1, pp. 147–157, 2009. DOI: 10.1016/j.compstruct.2008.02.014.
[32] T. Kant and K. Swaminathan, Estimation of transverse/interlaminar stresses in laminated composites – A selective review and survey of current developments, Compos. Struct., vol. 49, no. 1, pp. 65–75, 2000. DOI: 10.1016/S0263-8223(99)00126-9.
[33] R. K. Kapania and S. Raciti, Recent advances in analysis of laminated beams and plates. Part II: vibrations and wave propagation, Aiaa J., vol. 27, no. 7, pp. 935–946, 1989. DOI: 10.2514/3.59909.
[34] A. Ammar, B. Mokdada, F. Chinesta, and R. Keunings, A new family of solvers for some classes of multidimensional partial differential equations encountered in kinetic theory modeling of complex fluids, J. Non-Newton. Fluid Mech., vol. 139, no. 3, pp. 153–176, 2006. DOI: 10.1016/j.jnnfm.2006.07.007.
[35] P. Ladevèze, Nonlinear Computational Structural Mechanics – New Approaches and Non-incremental Methods of Calculation. Springer, New York, NY; 1999. DOI: 10.1007/978-1-4612-1432-8
[36] O. Allix and P. Vidal, A new multi-solution approach suitable for structural identification problems, Comput. Methods Appl. Mech. Eng., vol. 191, no. 25–26, pp. 2727–2758, 2002. DOI: 10.1016/S0045-7825(02)00211-6.
[37] P.-A. Boucard, D. Néron, and N. Relun, Time-space PGD for the rapid solution of 3D nonlinear parametrized problems in the many-query context, Int. J. Num. Meth. Eng., vol. 103, pp. 275–292, 2015. DOI: 10.1002/nme.4893.
[38] B. Bognet, F. Bordeu, F. Chinesta, A. Leygue, and A. Poitou, Advanced simulation of models defined in plate geometries: 3D solutions with 2D computational complexity, Comput. Methods Appl. Mech. Eng., vol. 201–204, pp. 1–12, 2012. DOI: 10.1016/j.cma.2011.08.025.
[39] P. Vidal, L. Gallimard, and O. Polit, Assessment of a composite beam finite element based on the proper generalized decomposition, Compos. Struct., vol. 94, no. 5, pp. 1900–1910, 2012. DOI: 10.1016/j.compstruct.2011.12.016.
[40] P. Vidal, L. Gallimard, and O. Polit, Composite beam finite element based on the proper generalized decomposition, Comput. Struct., vol. 102–103, pp. 76–86, 2012. DOI: 10.1016/j.compstruc.2012.03.008.
[41] P. Vidal, L. Gallimard, and O. Polit, Proper generalized decomposition and layer-wise approach for the modeling of composite plate structures, Int. J. Solids Struct., vol. 50, no. 14–15, pp. 2239–2250, 2013. DOI: 10.1016/j.ijsolstr.2013.03.034.
[42] H. Tertrais, R. Ibanez, A. Barasinski, C. Ghnatios, and F. Chinesta, On the proper generalized decomposition applied to microwave processes involving multilayered components, Math. Comput. Simulat., vol. 156, pp. 347–363, 2019. DOI: 10.1016/j.matcom.2018.09.008.
[43] A. Nouy, A priori model reduction through proper generalized decomposition for solving time-dependent partial differential equations, Comput. Methods Appl. Mech. Eng., vol. 199, no. 23–24, pp. 1603–1626, 2010. DOI: 10.1016/j.cma.2010.01.009.
[44] F. Chinesta, A. Ammar, A. Leygue, and R. Keunings, An overview of the proper generalized decomposition with applications in computational rheology, J. Non-Newtonian Fluid Mech., vol. 166, no. 11, pp. 578–592, 2011. DOI: 10.1016/j.jnnfm.2010.12.012.
[45] M. H. Malik, D. Borzacchiello, J. V. Aguado, and F. Chinesta, Advanced parametric space-frequency separated representations in structural dynamics: A harmonic-modal hybrid approach, Comp. Rendus Mécaniq., vol. 346, no. 7, pp. 590–602, 2018. DOI: 10.1016/j.crme.2018.04.005.
[46] A. Ammar, B. Mokdad, F. Chinesta, and R. Keunings, A new family of solvers for some classes of multidimensional partial differential equations encountered in kinetic theory modeling of complex fluids, J. non-Newtonian Fluid Mech., vol. 139, no. 3, pp. 153–176, 2006. DOI: 10.1016/j.jnnfm.2006.07.007.
[47] P. Vidal, L. Gallimard, and O. Polit, Composite beam finite element based on the proper generalized decomposition, Comput. Struct., vol. 102-103, pp. 76–86, 2012. DOI: 10.1016/j.compstruc.2012.03.008.
[48] S. Kapuria, P. C. Dumir, and N. K. Jain, Assessment of zigzag theory for static loading, buckling, free and forced response of composite and sandwich beams, Compos. Struct., vol. 64, no. 3–4, pp. 317–327, 2004. DOI: 10.1016/j.compstruct.2003.08.013.
[49] P. Vidal and O. Polit, Vibration of multilayered beams using sinus finite elements with transverse normal stress, Compos. Struct., vol. 92, no. 6, pp. 1524–1534, 2010. DOI: 10.1016/j.compstruct.2009.10.009.
[50] W. Zhen and C. Wanji, An assessment of several displacement-based theories for the vibration and stability analysis of laminated composite and sandwich beams, Compos. Struct., vol. 84, no. 4, pp. 337–349, 2008. DOI: 10.1016/j.compstruct.2007.10.005.
[51] X. Li and D. Liu, Generalized laminate theories based on double superposition hypothesis, Int. J. Numer. Methods Eng., vol. 40, no. 7, pp. 1197–1212, 1997. DOI: 10.1002/(SICI)1097-0207(19970415)40:7<1197::AID-NME109>3.0.CO;2-B.
[52] M. Aydogdu, Vibration analysis of cross-ply laminated beams with general boundary conditions by Ritz method, Int. J. Mech. Sci., vol. 47, no. 11, pp. 1740–1755, 2005. DOI: 10.1016/j.ijmecsci.2005.06.010.

Appendix: A Calculation parameters for the numerical tests

Table A1. Parameters of the finite element models using ANSYS.

Numerical test	L (m)	S	Relative element size	Number of elements
Isotropic beam	10	5	$L/100$	2000
Symmetric laminated composite beam	1	2	$L/125$	8000
	1	5	$L/125$	3375
	1	10	$L/125$	1875
	1	20	$L/125$	1000
Anti-symmetric laminated composite beam	1	2	$L/125$	8000
	1	5	$L/125$	3250
	1	10	$L/125$	1750
	1	20	$L/125$	1000
Three layer sandwich beam	1	2	$L/125$	8000
	1	5	$L/125$	3250
	1	10	$L/125$	1750
	1	20	$L/125$	875
Unsymmetric sandwich beam	1	4	$L/384$	36864
	1	10	$L/720$	51840
Boundary condition analysis	1	5	$L/125$	3375

Table A2. PGD calculation parameters.

Numerical test	L (m)	S	n_x	n_z (per layer)	$f_{\min}$ (Hz)	$f_{\max}$ (Hz)	Δf (Hz)	N
Isotropic beam								
N analysis	10	5	50	10	40	800	1	–
Spatial mesh analysis	10	5	–	–	40	450	1	10
Load position analysis	10	5	50	10	40	450	1	10
Symmetric laminated composite beam	1	2	100	[4,8,4]	600	4200	1	30
	1	5	100	[4,8,4]	500	5000	1	30
	1	10	100	[4,8,4]	300	4500	1	30
	1	20	100	[2,4,2]	100	4000	1	30
Anti-symmetric laminated composite beam	1	2	100	[8,8]	600	3000	1	50
	1	5	100	[8,8]	300	4000	1	50
	1	10	100	[8,8]	200	4200	1	30
	1	20	100	[4,4]	100	4000	1	30
Three layer sandwich beam	1	2	100	[1,2,1]	500	5000	1	30
	1	5	100	[1,2,1]	500	5000	1	30
	1	10	100	[1,2,1]	450	5500	1	30
	1	20	100	[1,2,1]	250	5500	1	40
Unsymmetric sandwich beam	1	4	100	[1,1,5,1,1]	50	600	1	30
	1	10	100	[1,1,5,1,1]	40	350	1	30
Boundary condition analysis								
FF	1	5	100	[2,2,2]	0.01	1	0.01	10
CC	1	5	100	[2,2,2]	0.01	0.5	0.01	10
SF	1	5	100	[2,2,2]	0.01	0.5	0.01	5
CS	1	5	100	[2,2,2]	0.01	0.5	0.01	5
SS	1	5	100	[2,2,2]	0.01	0.5	0.01	10
CF	1	5	100	[2,2,2]	0.01	0.3	0.01	10

Note: the load frequency range considered in the PGD performance is $[\omega_{\min}, \omega_{\max}]$, with $\omega_{\min} = 2\pi f_{\min}$ and $\omega_{\max} = 2\pi f_{\max}$.